AXISYMMETRIC BEM FORMULATION FOR CONTACT-INDUCED CRACK PROPAGATION ANALYSIS: FURTHER INDENTATION TESTS

Luiz Alkimin de Lacerda
LACTEC – Instituto de Tecnologia para o Desenvolvimento,
Centro Politécnico da UFPR, Cx.P. 19067, Curitiba – PR, Brazil.
alkimin@lactec.org.br

Luiz Carlos Wrobel
Brunel University, Department of Mechanical Engineering,
Uxbridge, Middlesex UB8 3PH, UK.
luiz.wrobel@brunel.ac.uk

Abstract. *Axisymmetric boundary element formulations for contact and fracture mechanics are employed for the simulation of indentation tests. The method combines a load-scaling boundary element technique for frictional contact analysis and a dual boundary element method (dual BEM) for axisymmetric crack propagation ones. The efficiency of these two techniques has been previously demonstrated. An efficient coupled formulation, capable of simulating contact-induced crack propagation while keeping proper equilibrium conditions in the frictional contact area, was recently presented. This coupling is briefly revisited in this paper. Aggregating the efficiency of the separate formulations is not straightforward and possible approaches are explained. The validity and efficiency of the proposed approaches are verified through several new indentation tests under different circumstances.*

Keywords*. Boundary element method, Contact, Axisymmetry, Crack propagation, Friction.*

1. Introduction

Indentation tests are commonly used for the assessment of material fracture properties. In particular, indentation of brittle solids by relatively hard spherical and flat-tipped indenters may induce the growth of cone cracks.

Two-dimensional and axisymmetric boundary element formulations for contact mechanics have been developed during the eighties by Andersson (1981) and Abdul-Mihsein et al. (1986), respectively. de Lacerda and Wrobel (2000) developed an efficient axisymmetric one, applicable to linear elastic materials, in which an incremental load-scaling technique is used to guarantee proper traction behaviour at the edge of the frictional contact area.

From the fracture mechanics point of view, only recently, a dual boundary element formulation for axisymmetric elasticity problems has been presented (de Lacerda and Wrobel, 2002). This particular technique is well suited for crack problems allowing the computation of stress intensity factors with great accuracy and the analysis of crack propagation problems also with great efficiency.

In the present work the coupling of the aforementioned frictional contact and dual fracture formulations is performed with the objective of modeling indentation tests. An algorithm for this coupling is proposed and the dual formulation is adapted to account for the incremental procedure. The keypoint in this development is to aggregate the efficiency of both formulations into the proposed algorithm. In this sense, the friction in the contact area brings some difficulties as well as requirements concerning the type of crack elements which must be added during propagation.

2. Contact and Crack Models

Consider a system of two or more elastic bodies in contact, in equilibrium under external loads and constraints. Problems involving contact can be categorized in different ways depending on characteristics such as the geometry of the contacting surfaces, presence of friction and loading history.

In non-conforming frictional contacts the final extent of the contact area is not known *a priori* and depends on the magnitude of the applied external forces. Furthermore, the presence of friction implies the development of shear stresses whose magnitudes may lead to relative tangential displacements at the contact interface, and which are also dependent on the load history. This load dependence of the analysis makes it nonlinear, requiring the subdivision of the external loads for its solution,

$$P^m = \sum_{k=1}^{m} \Delta P^k = P^{m-1} + \Delta P^m \tag{1}$$

where P^m represents all external loads at the final stage. As a consequence of this load discretization, displacements and tractions at the bodies are also subdivided

$$u_j^m(x) = u_j^{m-1}(x) + \Delta u_j^m(x)$$
$$t_j^m(x) = t_j^{m-1}(x) + \Delta t_j^m(x) \tag{2}$$

where it is clear that each load increment ΔP^k results in changes to the displacement and traction fields corresponding to Δu_j^k and Δt_j^k, respectively. Neglecting body forces and considering this subdivision, the following incremental boundary integral equation can be derived,

$$C_{ij}(\xi)\Delta u_j^k(\xi) = \int_\Gamma \lambda U_{ij}(\xi,x)\Delta t_j^k(x)d\Gamma - cpv\int_\Gamma \lambda T_{ij}(\xi,x)\Delta u_j^k(x)d\Gamma \tag{3}$$

where $U_{ij}(\boldsymbol{\xi},\boldsymbol{x})$ and $T_{ij}(\boldsymbol{\xi},\boldsymbol{x})$ are the displacement and traction fundamental solutions at a field point $\boldsymbol{x}$ due to a unit load applied at a boundary point $\boldsymbol{\xi}$, the free term $C_{ij}(\boldsymbol{\xi})$ is dependent on the geometry at $\boldsymbol{\xi}$, $\Delta u_j^k(\boldsymbol{x})$ and $\Delta t_j^k(\boldsymbol{x})$ are the displacement and traction increments over the boundary Γ, and the sign on the second integral (*cpv*) indicates Cauchy Principal Value. In axisymmetric analyses $i, j = r, z$ and $\lambda = 2\pi r_x$, with r and z being the radial and axial coordinates, respectively, and r_x being the radial distance from the field point $\boldsymbol{x}$ to the axis of symmetry z.

Subdividing Γ into a series of boundary elements and choosing appropriate functions to represent the displacements and tractions at these elements, Eq. (3) can be used to build a system of equations, which together with boundary and contact equilibrium and compatibility conditions, is solved to obtain unknown variables all over the boundaries.

Assuming m as the number of load steps, m sets of results for $\Delta u_j^m(\boldsymbol{x})$ and $\Delta t_j^m(\boldsymbol{x})$ need to be calculated. At each step k the contact conditions will depend on the total contact profile at the previous step $k-1$.

Multiple steps ($m > 1$) are essential for an accurate analysis. Different criteria can be used to define the load increments ΔP^k. Here, node to node contact elements and a load scaling technique are used to calculate these increments. The basic idea of this technique is to use a linear extrapolation function to obtain a very close to zero normal traction value at the pair of nodes at the edge of the contact area.

At each load step, an iterative procedure is necessary to find the correct partitioning of stick and slip regions. In this iteration process compatibility contact equations are changed appropriately.

Notice from Eq. (3) that the integrations do not change in the incremental process, only the compatibility contact equations may be modified. An LU linear system solver (L is a lower-triangular square matrix with unity diagonal elements, and U is an upper-triangular square matrix) is quite attractive for the load-scaling scheme where trial loads are employed (provided the size of the problem is not a restriction to the application of $O(N^3)$ solvers). However, to perform a new LU decomposition every time a compatibility equation is modified is a very expensive task Fortunately, these modifications are usually very small compared to the number of equations in the system and this feature gives room to the application of special algorithms to speed-up the analysis (de Lacerda and Wrobel, 2000). The suitability of such scheme to crack propagation analysis is investigated.

The dual BEM is a very attractive method to model fracture mechanics problems because of its accuracy and easy `re-meshing' on crack propagation analysis. The method basically consists on the simultaneous application of the displacement and traction boundary integral equations to the crack boundaries (Portela et all, 1991), giving rise to a mathematically well-posed formulation.

Recently, traction equations have been derived for axisymmetric elasticity (de Lacerda and Wrobel, 2001). Without loss of generality, the traction boundary integral equation is also written in incremental form,

$$\frac{1}{2}\Delta t_i^k(\xi) = m_l cpv\int_\Gamma \lambda D_{ilj}(\xi,x)\Delta t_j^k(x)d\Gamma - m_l hpv\int_\Gamma \lambda S_{ilj}(\xi,x)\Delta u_j^k(x)d\Gamma \tag{4}$$

where the collocation point $\boldsymbol{\xi}$ is on a smooth part of the boundary Γ, m_k are the components of the normal vector at $\boldsymbol{\xi}$, $D_{ikj}(\boldsymbol{\xi},\boldsymbol{x})$ and $S_{ikj}(\boldsymbol{\xi},\boldsymbol{x})$ are known functions of derivatives of $U_{ij}(\boldsymbol{\xi},\boldsymbol{x})$ and $T_{ij}(\boldsymbol{\xi},\boldsymbol{x})$, and the sign on the second integral (*hpv*) indicates Hadamard Principal Value.

Crack boundary conditions are usually traction free and that may well be the case for the increments of growing cracks. Still, imposing these conditions is not straightforward in an incremental formulation, and details of these procedures are thoroughly explained in the next section. The use of different element types rather than simple traction free ones is investigated.

After the boundary discretization, Eqs. (3) and (4) are applied at crack nodal points, one on each side of the crack. At non-crack boundaries only Eq. (3) is applied. A discretized system of equations is obtained where integrals over each element must be computed. Two types of integrations will appear: non-singular and singular. The first ones are computed using Gauss quadrature and the second requires different treatments, depending on which kernel of each equation is being integrated.

An accurate evaluation of stress intensity factors is essential for crack trajectory simulations. Here, the modified crack closure integral method (Rybicki and Kanninen, 1977) is adopted for its simplicity, speed and good level of accuracy. The method is based on an approximate evaluation of the crack closure integrals, proposed by Irwin (1957).

3. Crack Propagation Model

Cracks will extend until stress intensity factors fall bellow the critical stress value K_T (toughness) of the material. Several criteria have been proposed to determine the direction in which cracks should propagate. Perhaps the most commonly used is the maximum principal stress criterion. It predicts that cracks will grow in a direction perpendicular to the maximum principal stress at their tip. With the knowledge of the stress intensity factor values K_I and K_{II}, this direction θ_c can be easily obtained. Fracture instability occurs at a crack tip when the maximum principal stress reaches the toughness magnitude K_T. Assuming that an equivalent mode *I* stress intensity factor K_{Ieq} is responsible for the fracture process, this condition is present when $K_{Ieq} > K_T$.

Once the directions are defined, crack increments are added to the system: a pair of elements for each extended crack. Their sizes are usually controlled as an increasing or decreasing function of the corresponding tip element size. Observe that the predicted angles θ_c do not take into account the length of the increments, so corrections are found necessary to adjust their orientations. This so-called prediction-correction technique is an iterative procedure which requires an efficient method for the solution of the system, since this process will be repeated a great number of times. LU decomposition and the dual boundary element method can also be efficiently used in this crack propagation procedure (Portela et al, 1991). Prior to the incrementation, all current coefficients of the system have been decomposed and properly stored. When cracks are incremented, a few extra rows and columns are added to the system and these new system coefficients are the only ones to be decomposed. Actually, they are decomposed as many times as the increment elements are adjusted during the iterations, searching for the best θ_c values.

It was seen that an LU solver can be efficiently used in contact and crack analyses. In combined problems such as contact-induced crack propagation, the algorithm for the solution must be simultaneously efficient. In this type of problem, before cracks start propagating, a certain amount of load has necessarily been applied. Consider this particular stage of the analysis, where *k* load steps have been applied and a certain number of iterations were performed to obtain the current contact status and overall solution. Let H_k denote the history of operations which transform the initial contact configuration into the current one (after *k* steps). As mentioned for the contact model, this history of changes provides a series of modifications on the solution which can be quickly evaluated. Moreover, reapplying this group of operations is an even faster procedure since much of the computation during the first time has been stored.

The LU decomposition of the new coefficients in the propagation algorithm is stored alongside the original decomposed matrix. It is worth remembering that, originally, the system contained contact conditions for the initial configuration. After the system solution, results will correspond to the initial contact status and a history of load increments and contact iterations must be applied to recover the current load stage P^k. Unfortunately, reapplying the operations H_k to the new slightly larger system is not sufficient to obtain the new results. These operations are likely to open the crack increments at load steps smaller than *k*, but somehow the increments must be kept closed until the fracturing moment when the amount of load P^k is reached. This task differentiates the present combined contact crack analysis from pure crack propagation ones, and overcoming this problem with efficiency is the key point of the algorithm. The approach used to solve this task is described in the next section, along with possible alternatives with advantages and disadvantages of each discussed.

Finally, the last step of the propagation algorithm corresponds to the angle adjustments of the crack increments. These corrections are necessary until a predefined tolerance is reached. This tolerance, which can be specified by the analyst, is the maximum allowed difference in degrees between the previous and the currently calculated direction of propagation (δ_θ). The smaller this value, the greater the number of angle iterations and time of analysis. If any of the increments is tilted, the former new decomposed coefficients are discarded along with the last set of results and the process is restarted from the assembling routine. The whole incrementing process is repeated until $K_{Ieq} < K_T$ at all crack tips. When all cracks are arrested by the toughness of the relevant material the analysis returns to the contact algorithm, possibly for further load incrementations and contact iterations.

4. Recovering the Current Load

At this point, cracks have grown and the number of unknowns in the system has increased proportionally to the number of extra elements. Basically, regarding the boundary conditions, elements can be of two types: simple boundary elements (fck - traction free crack elements) with two unknown values per node, or contact boundary elements (cck - contacting crack elements) with an additional two unknowns per node. The first type has one-half of the number of unknowns compared to the second and this difference, in terms of computational speed, becomes evident as the system is progressively expanded with the crack growth. Therefore, its use should be preferred, however, inserting it in the proposed incremental contact model is much more complicated. Tractions would have to be prescribed at these elements in order to keep increments closed up to the last step before their opening. These values are not known and would have to be calculated in a post-processing level using results from the unincremented system. Furthermore, adapting these conditions to the external load scaling process and elaborating a book-keeping format for the future

crack increments to be added to the system, are enough reasons to discourage the use of this type of element in the present method. Nevertheless, a less accurate approach is later discussed where these elements are used with some success. On the other hand, contact elements have been implemented with the load scaling and history of results in mind, and keeping the gaps closed at any stage is as simple as defining the elements to be in stick mode.

For simplicity, consider the single crack propagation case in Fig. 1, although the following approach is general and extendable to multiple crack analysis. The top row of Fig. 1 shows a sketch of the crack growing process. The load is incremented ($a \rightarrow b$) until the value P^k is reached, where the equivalent mode I stress intensity factor is greater than the toughness of the material. Next, the load is kept constant and the crack is extended ($b \rightarrow c$) perpendicular to the maximum principal stress direction. In Fig. 1*c*, the mesh has two more contact elements, and new rows and columns are added to the system. After the decomposition of these new coefficients, the system is solved providing a solution vector $\boldsymbol{S_0}$ which represents the situation in Fig. 1*d*. The objective is to obtain the solution $\boldsymbol{S_k}$ which corresponds to the load P^k with the new crack increment (Fig. 1*f*). In the new system, it is necessary that the new pair of elements behave as in stick mode until the crack opening stage, as depicted in the bottom row of Fig. 1. The computation of $\boldsymbol{S_k}$ is better visualized if performed in two steps: First, the solution $\boldsymbol{S_0}$ is transformed into an intermediate solution corresponding to Fig. 1*e*, through a series of known operations H_k. Secondly, the crack increment is simply released from stick mode ($e \rightarrow f$) and contributions from this event are added to the intermediate solution giving $\boldsymbol{S_k}$.

In practice, these two steps are independent from each other and can be simplified into a single faster one. The crack increment is set as a separate contact pair with zero gap in the first place, with compatibility conditions provided from post-processed stresses $t_j^{k,b}$ in the uncracked system in Fig. 1b,

$$\Delta \boldsymbol{t}_j^k = -\boldsymbol{t}_j^{k,b} \tag{5}$$

After decomposition and system solution, a different result for $\boldsymbol{S_0}$ is obtained and the simple fast application of H_k over this system, plus extra contact iterations if the status changes between configurations *b* and *c*, gives the solution $\boldsymbol{S_k}$. Apart from numerical errors, traction-free conditions $t_j^{k,f} = 0$ at the crack increment is a result within $\boldsymbol{S_k}$.

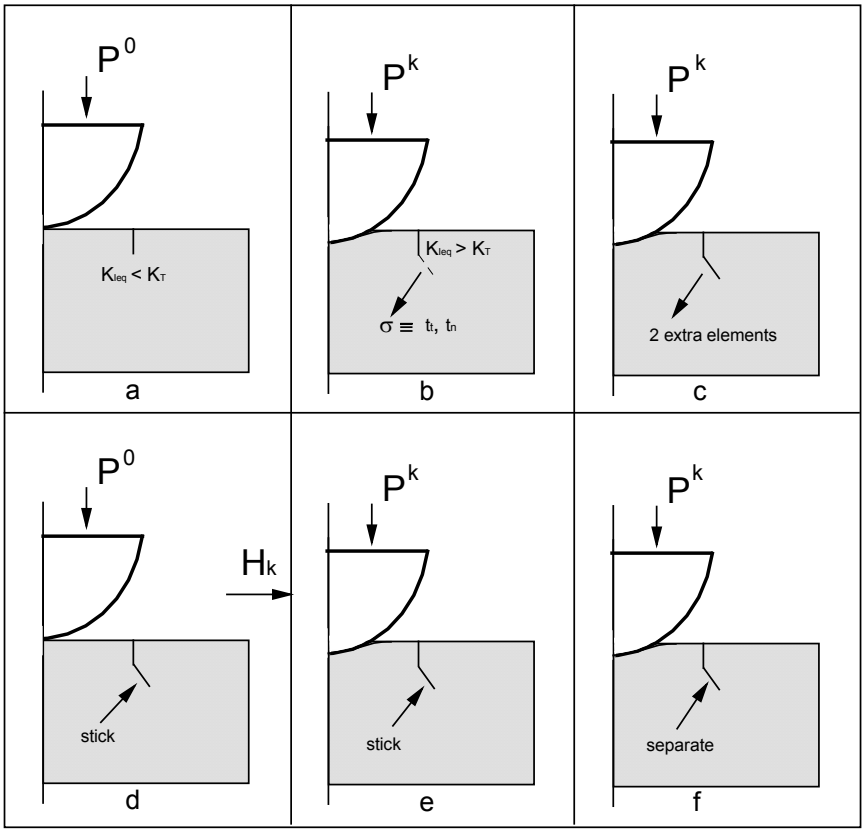

Figure 1. Steps during crack propagation.

The load scaling technique is based on calculating the load P^k which results in near zero normal tractions at the edge of the contact area. With the crack propagation, it is normal that changes on the contact stresses will occur. The normal traction values at the edge will no longer be zero, however the differences are normally negligible compared to the stresses in the vicinity.

4.1. Crack increments with simple boundary elements

Simple boundary elements (fck) can still be used for the increments discretization in a different approach. In this case, the previous history of increments and iterations H_k is completely discarded. A new incremental contact loading history is initiated and processed until the target load is reached. Recalculating the whole history can be very time-consuming, specially because it has to be re-done after every correction. Still, it is much faster than decomposing and solving the whole system with updated contact conditions. Compared to the formal approach with contact elements, the present one may even be faster if a large number of crack increments is added to the system. The main problem of this approach is the presence of the open crack increments at the beginning of the iterations, which does not occur in practice. For this reason, it is expected that the frictional contact stresses will be different from the real ones (frictionless analyses should not be affected). Another issue which may be influenced by this approach is the crack trajectories. These matters are investigated in the following examples.

It may be claimed that, if the previous approach cannot guarantee correctness of the frictional stresses, then applying multiple load steps would not be essential. Instead, just a single load step could be used as an alternative, speeding up the analysis. This extra approximation certainly yields less accurate frictional contact stresses, compared to the multiple steps case.

5. Contact-Induced Crack Propagation Analysis

A number of indentation tests were numerically simulated to verify the accuracy and efficiency of the proposed formulation. Results are compared with simple theoretical formulae, when available, and with numerical results from previous simulations by other authors.

Three types of axisymmetric indenters are used in the numerical tests: a sphere (sph), a machined sphere (ms) and a cylinder (cyl). The first indenter has a radius of 1.98 mm and produces a non-conforming type of contact, with an increasing contact area as the load is augmented. The second indenter has the same radius and a flat base of 1 mm radius. The last indenter has a height also equal to 1.98 mm, and the same contacting area as the machined sphere, a circular base with 1 mm radius. The same material was employed for the three indenters – Tungsten carbide with Young's modulus of 614 GPa and Poisson's ratio equal to 0.22. The cracked specimen is an axisymmetric monolith, with radius and height equal to 20 mm. These dimensions were verified to be sufficiently large to avoid boundary influences over the propagating cracks. Three types of brittle materials were tested and their properties, including their fracture toughness, are presented in Tab. 1. In the contact area, nondimensional friction values of 0.05, 0.1, 0.2 and 0.3 were employed, besides some frictionless analyses.

Table 1. Monoliths material properties.

Material	*Soda-lime glass*	*Silicon Nitride*	*Fused silica*
Young´s modulus (Mpa)	69000	335000	70000
Poisson´s ratio	0.21	0.27	0.14
Fracture toughness (MPa $m^{1/2}$)	0.75	3.9	1.9

In the first validation test, the machined spherical indenter is pressed against the three types of monolith and a further, hypotetical one, with Poisson's ratio equal to 0.4 and an arbitrary Young's modulus. The contact is assumed to be frictionless, and a tiny crack c=10 μm long is imposed normal to the top surface of the monolith, distant from the axis of symmetry by r_0=1.1 mm. A total of 213 linear elements were used for the model discretization, with 10 along the initial crack (5 on each side) and 40 along each contacting surface. A 10 KN load was applied in a single step, and a total of 80 crack increments were allowed to propagate. As expected, cone cracks were formed as shown in Fig. 2. Note the different angles they make with the horizontal direction, which increase in an inverse proportion to the Poisson's ratio. The angle obtained in the case of the soda-lime glass monolith is approximately the same reported by Kocer and Collins (1997), while all the others match previously reported values (Bush, 1999).

The second set of tests includes a comparison between the two flat base indenters, for different friction values. The boundary element mesh was identical to the previous case, and the monolith material used was soda-lime glass. In the crack trajectories in Fig. 3, the angle of propagation was the same as before for the different combinations. However, it is interesting to notice that the trajectories are slightly offset from each other. This effect can be attributed to the influence of friction and the indenter geometry at the onset of the propagation. In the machined indenter case, the crack tends to find the cone angle before the cylindrical indenter case, *i.e.* with a smaller amount of applied load. The effect of friction is to keep the initial crack faces in contact, with a larger mode II stress intensity factor required for the initial development of the crack, as expected.

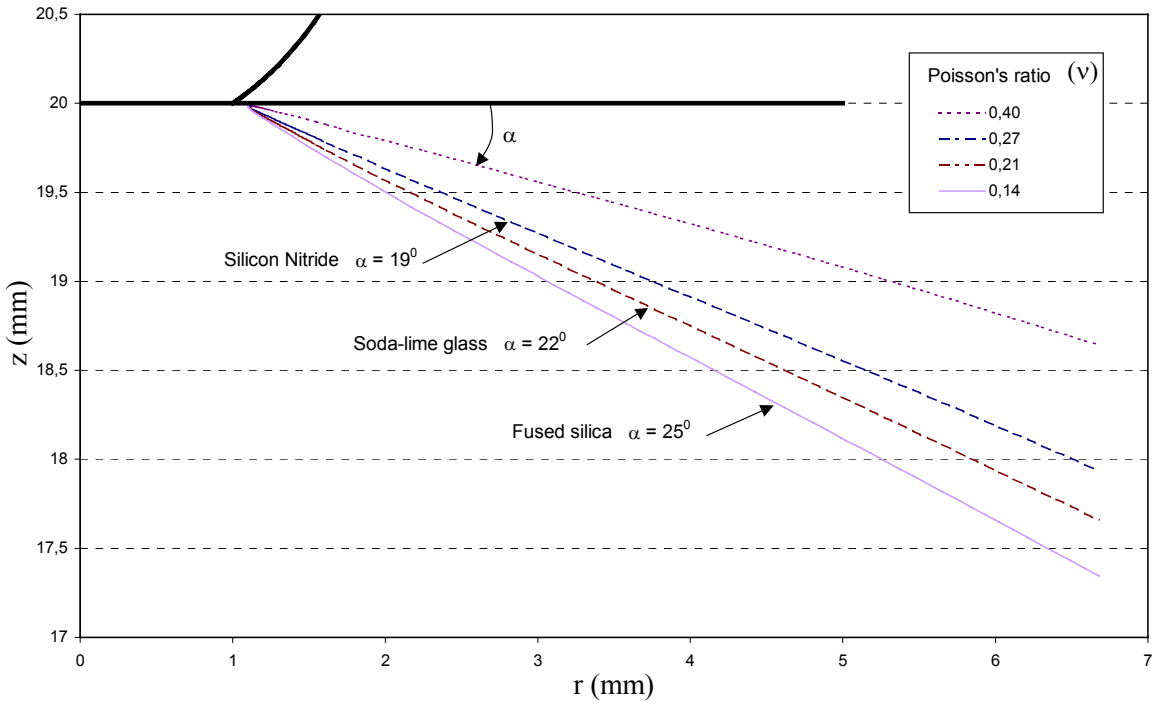

Figure 2. Cone angles formed during indentation of different materials.

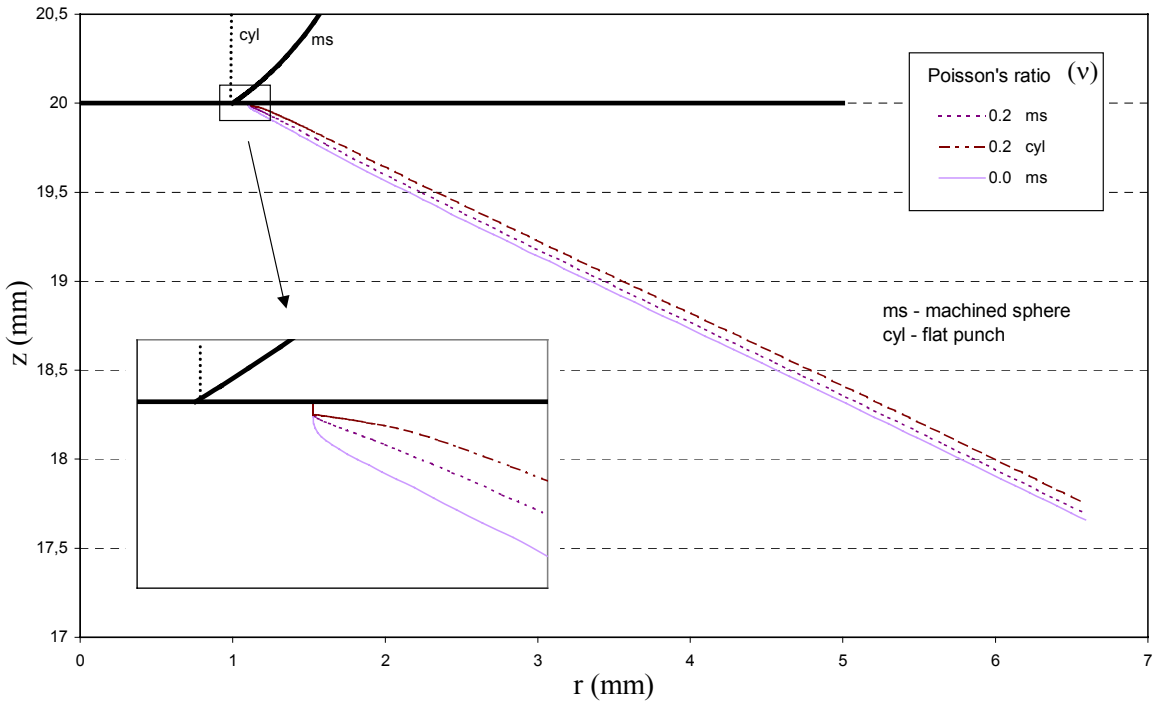

Figure 3. Effect of friction and indenter type on crack propagation.

The two flat indenters are also used to simulate the correlation between the applied load (P) and the base radius (R) of the cone crack, for the soda-lime monolith. The following expression is valid when R is sufficiently larger than the indenter radius (Lawn, 1993),

$$P^2 = \alpha R^3 \tag{6}$$

where α is a constant depending on the Poisson's ratio and fracture toughness of the cracked specimen. In Fig. 4, results for both indenters with frictionless contact conditions, and the cylindrical indenter with friction μ =0.05, compare well

with the asymptotic expression (6) in the specified range. Notice that the cylindrical indenter without friction appears to be in closer agreement, but although the other two results seem to be slightly outside, their slope is very similar to the expected one. This behaviour matches the observations in Fig. 3, where the cones are slightly offset. At the beginning of propagation, a 'pop in' effect can be observed. This phenomenon is well reported in the literature and corresponds, in Fig. 4, to the gaps between data at small values of R. Another point in agreement with observations in Fig. 3 is that a higher load was needed to initiate the propagation for the machined sphere, and an even higher one for the cylinder with friction, compared to the cylinder without friction. In fact, a much higher load was needed for the cylinder with friction, resulting in a larger 'pop-in' effect.

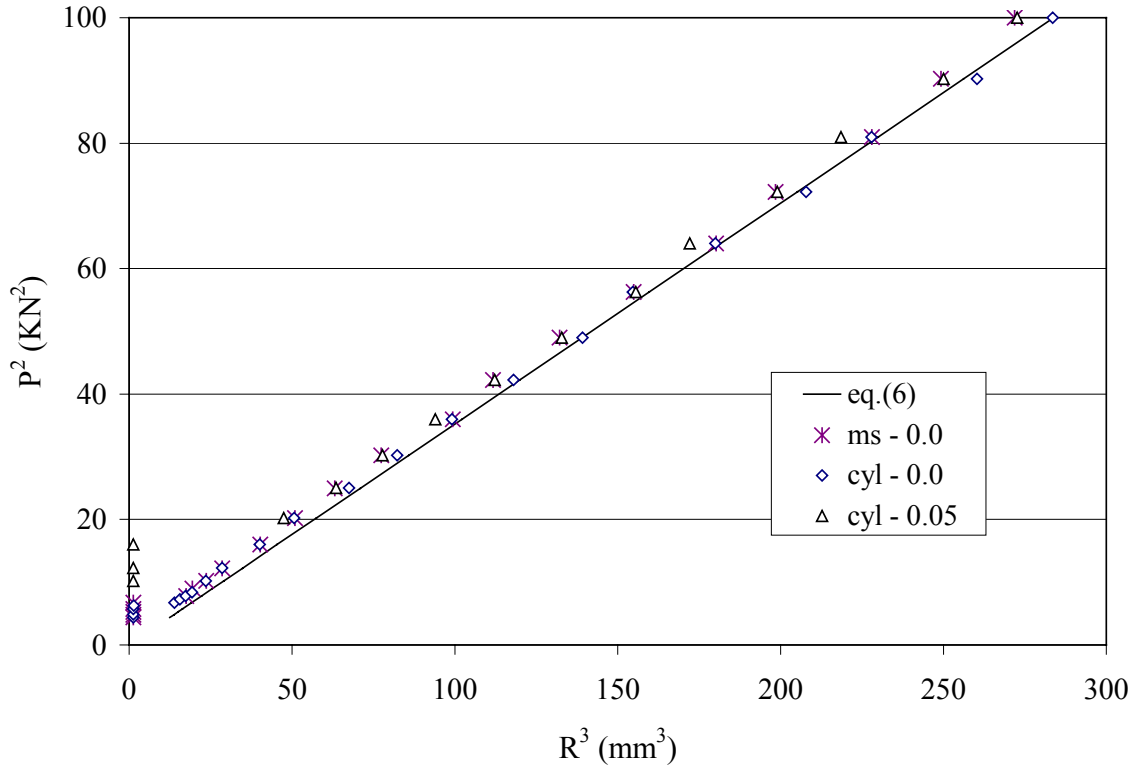

Figure 4. Relation between applied load and cone crack base radius for the conforming type of contact.

This behaviour is clarified in Fig. 5, which shows a plot of the normalized strain energy release rate as a function of crack length, following Lawn (1993) and Mauginot and Maugis (1985), for different values of the contact friction parameter. Two sets of curves are presented, for $r_0/a = 1.1$ and $r_0/a = 1.3$, where a is the cylinder radius and r_0 is the distance between the crack and the axis of symmetry. Although plots were only produced for a single load case, higher or lower indentation loads would simply shift the curves upwards or downwards, respectively (Mauginot and Maugis, 1985). The first crossing points between the curves and the stability line $G/2G_0 = 1$ (G_0 is the fracture surface energy) indicate the normalized crack length necessary to initiate propagation. It is clear that, in both cases, this length must be greater as friction increases. Alternatively, for a fixed crack length, increasing friction means that a higher load would be required to initiate propagation. It can be observed in Fig. 5 that all curves present two peaks, a characteristic feature of cylindrical punches, and that the amplitude of the first peak increases with the ratio r_0/a, in agreement with the results of Mauginot and Maugis (1985).

Figure 6 presents the accumulated CPU time (on a Pentium III-750/128Mb) for the propagation of eighty crack increments in the soda-lime monolith, induced by the cylindrical indenter, under different circumstances. It is clear that applying all the load in one single step (total load) is faster than using several steps. Therefore, in a conforming type of contact, this approach should be preferred if only the crack trajectory is sought. If a correlation between load and crack size is required, then load steps are necessary. In this case, it can be seen that the numerical procedures are much more time consuming when friction is considered. The main reasons are the greater number of contact iterations to define the stick-slip partition, and the longer time needed to compute the operations H_k to obtain the solution at the k-th load step. Another factor that can be observed is the influence the crack increment angle error tolerance (δ_θ) has on the CPU time. An analysis with an error tolerance of 3º is approximately twice faster than using 1º. This factor can be verified in the insert to Fig. 6, where a larger number of crack (angle) iterations are needed for the 1º case. This figure also shows that, after a certain number of increments, the number of crack iterations reduces to nearly one. This happens when the crack finds its straight direction of propagation

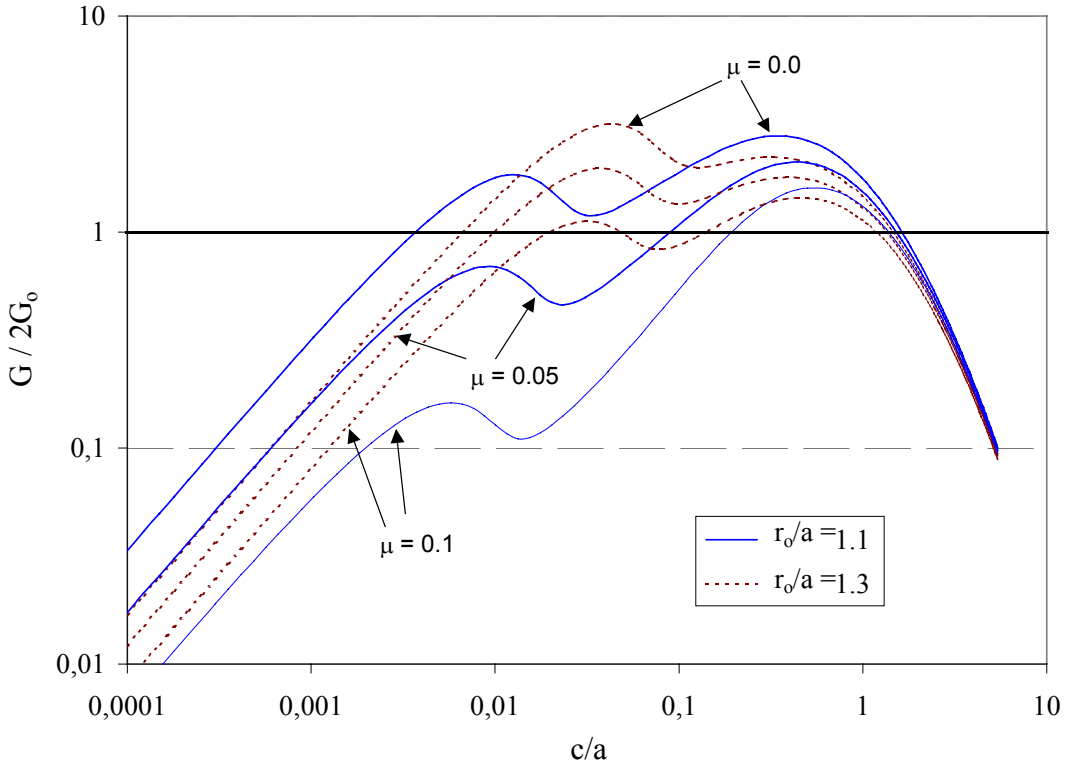

Figure 5. Cylindrical punch. Normalized strain energy release rate against c/a for two starting locations of the crack and different contact friction values.

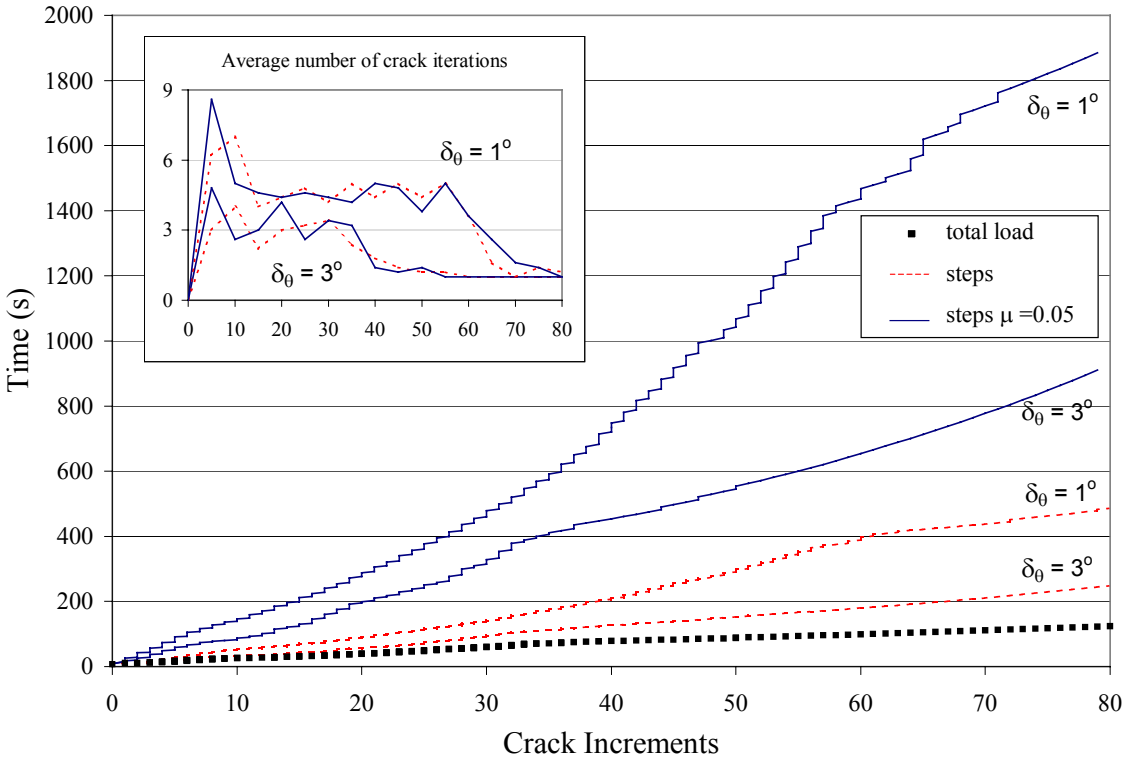

Figure 6. Influence of friction, crack angle tolerance iteration and number of load steps on the performance of the algorithm.

Results for the non-conforming indentation test of a Silicon Nitride monolith block are depicted in Fig. 7, alongside theoretical and experimental trend lines. In this test, the initial crack is 8 μm long and 0.351mm distant from the axis of symmetry. The dual BEM results for the indenter load (P) versus the crack length (C) seem to converge to the

theoretical far-field relation. However, as previously observed by, the numerical results deviate from the experimental ones (Bush, 1999; Lee et all, 1997) as a result of plastic deformation within the indenter. Two regions of unstable crack growth at the onset of propagation were detected in this test. The applied load was never reduced during indentation, and this explains the gaps between data indicated by these regions. The first gap is between the initial crack location (dashed line) and the initial marks of the two presented results. The second gap is between the initial data marks and the fourth mark of each result. The two regions together correspond to the 'pop-in' effect commonly observed in experimental tests. It can be seen that the introduction of friction in this test was not significant at all. Neither the crack trajectories nor the minimal load for the 'pop-in' were substantially different. The minimum load necessary to initiate crack propagation was found to be P=1.59 KN, which is quite close to experimental observations (Lee et all, 1997), even though the initial crack size (8 μm) may not be the most appropriate and the formulation is not particularly well suited for this analysis, due to the absence of plasticity.

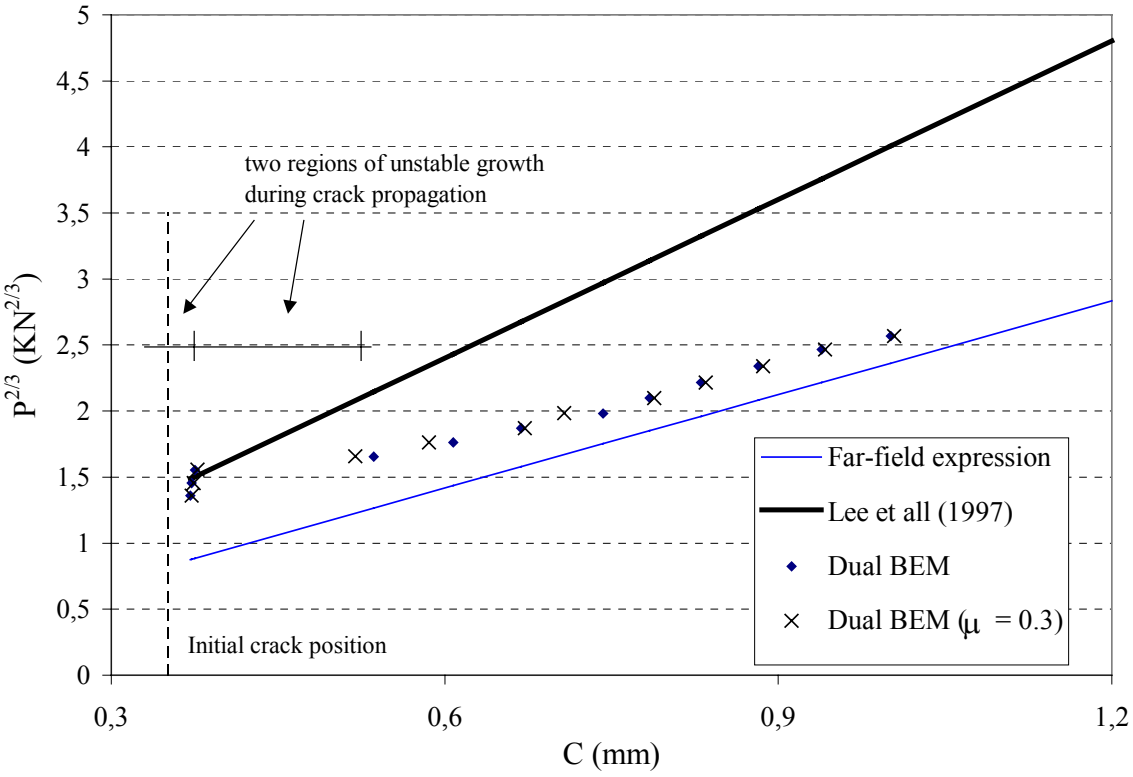

Figure 7. Relation between applied load and cone crack length on the spherical indentation.

The accumulated CPU times for the propagation of thirty-six crack increments in the previous non-conforming test are shown in Fig. 8. An angle error tolerance δ_θ=1º was adopted, and two types of crack elements were used to model the system: contacting crack elements (cck) and contact-free crack elements (fck). As expected, the use of fck elements for crack growth speeds up the analysis, since they involve a smaller number of unknowns. The load-scaling technique is used in this test, and it can also be seen that the introduction of friction delays the analysis, whatever type of crack elements are employed. The crack trajectories for the cases analysed are shown in the insert to Fig. 8. Neither the friction in the contact area, nor the type of crack element, seem to affect the crack path. Three zones are indicated in this figure. In the first, the curves are nearly horizontal, meaning that only a small number of contact and crack direction iterations are necessary. This effect continues until the crack growth reaches the compression area formed in the monolith. The second zone corresponds to the deviation of the propagating crack to avoid the compressive area. In this process, a larger number of crack direction iterations is needed, resulting in a steeper curve. In the third zone, the crack reaches its straight path, and the curve slope increases as more crack increments are added to the system.

The frictionless cases needed not be incremental, and a single load step should be sufficient for the analysis. As for the added crack elements, the fck type of elements is also appropriate. On the other hand, for frictional problems, the applied indenter load has to be incremental, and fck elements cannot produce a completely correct result as can be seen in Fig. 9. A friction value of μ =0.05 was used in the same non-conforming test, and no differences were noticed for the normal contact tractions.

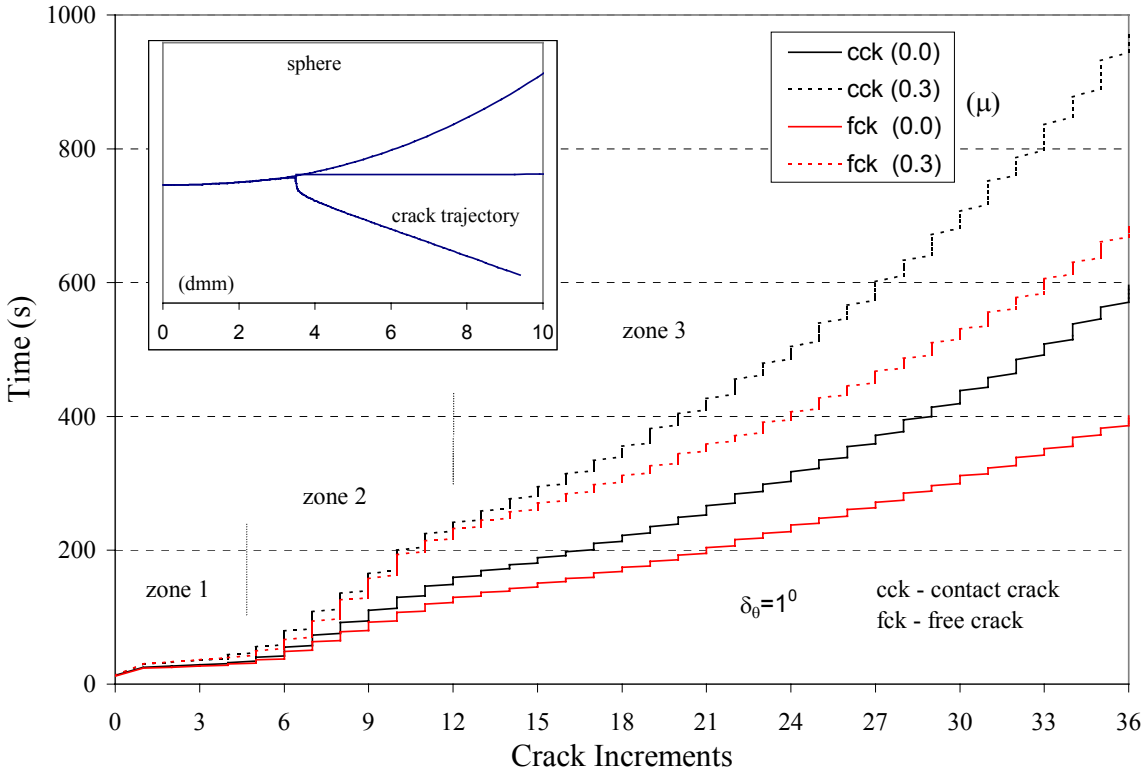

Figure 8. Influence of friction and choice of crack element increment on the performance of the algorithm.

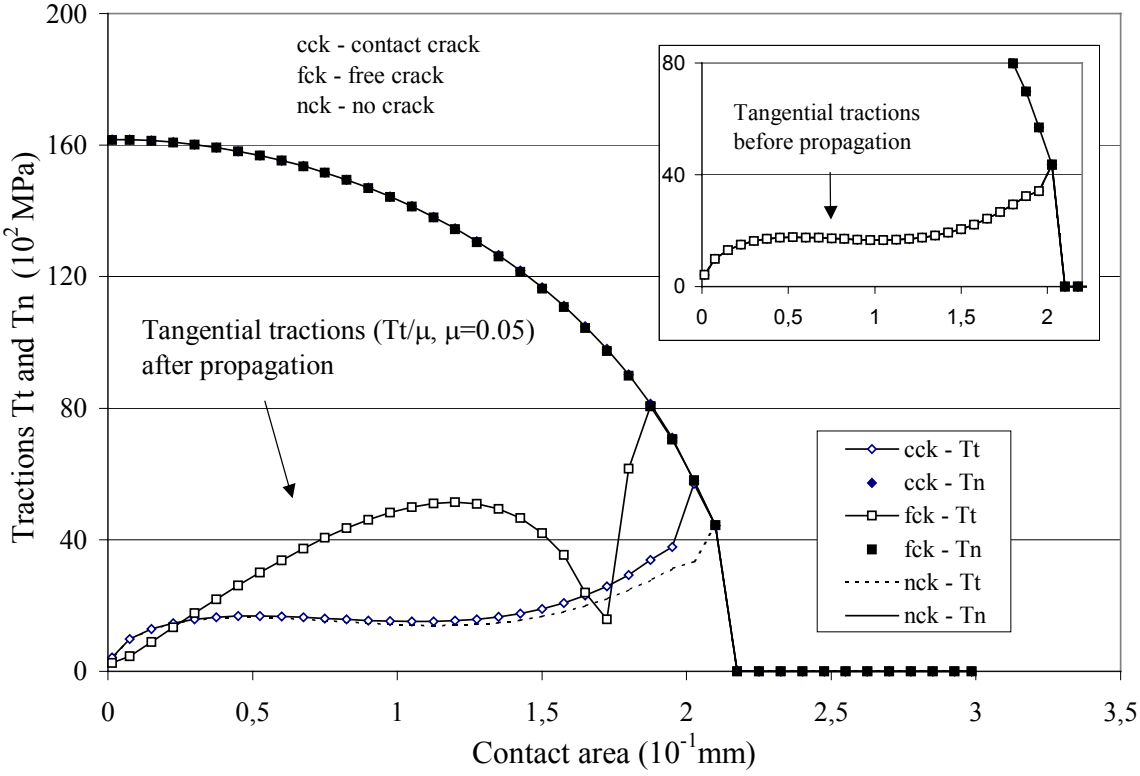

Figure 9. Influence of the choice of crack element increment on the tangential tractions development.

Prior to the crack propagation, tangential tractions were the same whether fck or cck elements were used. After the initial crack propagation, the analysis with cck elements closely matches the same contact problem without the crack

(nck). However, when fck elements are used, the tangential traction values are very different from the previous results. This behaviour was expected as reported in the previous section, despite the lack of plasticity in the analysis.

6. Conclusions

Boundary element algorithms for the analysis of contact-induced crack propagation problems have been developed. For this purpose, axisymmetric formulations for contact and crack analysis were coupled in an incremental manner. Conforming and non-conforming frictional contact are considered and the dual boundary element method is used in the crack modelling, allowing the analysis of crack propagation in a faster and elegant manner.

An efficient approach is employed to retrieve the solution with speed and accuracy. Once the initial system is solved, contact iterations are quickly performed to obtain the extension of the contact area and the stick-slip partition. For the crack formulation the original system is mantained and enlarged as the crack elements are added to the problem. The initial system decomposition and the contact history of iterations are also accounted for the computation of the solution after every crack increment.

The influence the choice of crack elements have on the solution speed and accuracy was demonstrated in the results. In general, the algorithms proved to be quite efficient, being able to simulate indentation tests in a few minutes.

The lack of plasticity in the present formulation seems to be the main reason for the mismatch in the load versus crack length results for the non-conforming indentation case. Future investigations will address this particular problem and the influence of plastic deformation due to high stress concentrations at the edges of flat punches. Finally, the algorithms proved to be quite efficient, and capable of accurately simulating indentation tests.

7. References

Abdul-Mihsein, M.J., Bakr, A.A. and Parker, A.P., 1986, “A boundary integral equation method for axisymmetric elastic contact problems”, *Computers & Structures*, **23**, 787-793.

Andersson T., 1981, “The boundary element method applied to two-dimensional contact problems with friction”, *Proceedings of the Third International Seminar on Boundary Element Methods*, Springer, Berlin.

Bush, M.B, 1999, “Simulation of contact-induced fracture”, *Engineering Analysis with Boundary Elements*, **23**, 59-66.

de Lacerda, L.A. and Wrobel, L.C., 2000, “Frictional contact analysis of coated axisymmetric bodies using the boundary element method”, *Journal of Strain Analysis for Engineering Design*, **35**, 423-440.

de Lacerda, L.A. and Wrobel, L.C., 2001, “The hypersingular boundary integral equation for axisymmetric elasticity”, *International Journal for Numerical Methods in Engineering*, **52**, 1337-1354.

de Lacerda, L.A. and Wrobel, L.C., 2002, “Dual boundary element method for axisymmetric crack analysis”, *International Journal of Fracture*, **113**, 267-284.

Irwin, G.R., 1957, “Analysis of stresses and strains near the end of a crack traversing a plate”*, Journal of Applied Mechanics*, **24**, 361-364.

Kocer, C. and Collins, R.E., 1997, “The angle of Hertzian cone cracks”, *Journal of the American Ceramic Society*, **81**, 1736-1742.

Lawn, B.R., 1993, *Fracture of Brittle Solids*, 2nd edition, Cambridge University Press, Cambridge.

Lee, S.K., Wuttiphan, S. and Lawn, B.R., 1997, “Role of microstructure in Hertzian contact damage in silicon nitride: mechanical characterization", *Journal of the American Ceramic Society*, **80**, 2367-2381.

Mauginot, R. and Maugis, D., 1985, “Fracture indentation beneath flat and spherical punches”, *Journal of Materials Science,* **20**, 4354-4376.

Portela, A., Aliabadi, M.H. and Rooke, D.P., 1991, “The dual boundary element method: effective implementation for crack problems”, *International Journal for Numerical Methods in Engineering*, **33**, 1269-1287.

Rybicki, E.F. and Kanninen, M.F., 1977, “A finite element calculation of stress intensity factors by a modified crack closure integral”, *Engineering Fracture Mechanics*, **9**, 931-938.